Analysis of solar potential in an urban area using LiDAR data: A case study of Belgium

Sharareh AKBARIAN, Australia

Arash JOUYBARI and Nina GRONDSTEIN, Sweden

Keywords: Light Detection and Ranging (LiDAR), Digital Surface Model (DSM), Shadow Detection, Solar Energy, Roof Surfaces.

SUMMARY

Nowadays, there has been an increasing demand for solar energy as a type of renewable energy because of the advantages such as providing heating and electricity, avoiding environmental pollutions, and utilizing the sustainable approach for the development of natural resources. Depending on the different positions of the sun at various times, different terrain topographies, and man-made objects, the amount of received solar energy will vary in different times and places. The goal of this study is to select the best roof surfaces regarding their suitability for photovoltaic systems' installations taking into account shadowing effects, size, aspect, and slope of the roof surfaces. The first step in the proposed method is to detect buildings by segmentation of a Digital Surface Model (DSM) derived from Light Detection and Ranging (LiDAR) data and classification of the segments as roof surfaces. The height information, slope, and aspect of the segments are utilized in the segmentation procedure. A shadow detection algorithm is developed to calculate the shadow coefficients for different roofs. Next, direct and diffuse solar radiations are obtained for each point on the selected roof and values of shadow are considered for them. A high-resolution LiDAR and optical data set from Belgium are considered to execute the proposed methodology. The results show the efficiency of the proposed method for solar potential determination of surfaces in preferable locations.

Analysis of solar potential in an urban area using LiDAR data: A case study of Belgium (10870)
Sharareh Akbarian (Australia), Arash Jouybari and Nina Grondstein (Sweden)

FIG e-Working Week 2021
Smart Surveyors for Land and Water Management - Challenges in a New Reality
Virtually in the Netherlands, 21–25 June 2021

Analysis of solar potential in an urban area using LiDAR data: A case study of Belgium

Sharareh AKBARIAN, Australia

Arash JOUYBARI and Nina GRONDSTEIN, Sweden

1. INTRODUCTION AND BACKGROUND

Due to an increase in environmental contaminations, the rising cost of fossil fuels, and global climate change caused by fossil fuel usage, renewable energy is becoming a viable solution in today's world (Assouline et al. 2017; Brito et al. 2017; Kassner et al. 2009). Thus, private investors and administrators have shown an interest in the deployment of renewable energy sources (Brito et al. 2017). There are various types of renewable energy sources such as solar, wind, water, and biomass. Solar energy is one of the best and most promising sources of renewable energies (Huang et al. 2012; Kassner et al. 2009). Solar radiation can be detected on the earth either direct or diffused form (Brito et al. 2017) Direct radiation is solar radiation traveling on a straight line from the sun down to the surface of the earth, while diffuse radiation is the sunlight that has been scattered by molecules and particles in the atmosphere. When the radiation is direct, the rays are all traveling in the same direction, an object can absorb them all at once. Therefore, shadows are only produced when direct radiation is blocked (Jochem et al. 2009a; Jochem et al. 2009b; Lukač et al. 2013; Redweik et al. 2013).

Photovoltaic systems turn solar radiation energy into heat energy and electricity (Bizjak et al. 2015). Thus, to use this technique some factors have to be considered. An installation should have a minimum size, a specific aspect, and a slope for the more efficient performance of the photovoltaic systems (Le et al. 2016; Margolis et al. 2017). Besides, shadowing effects, e.g. caused by higher buildings or vegetation in the surrounding, have to be taken into account, since the shadow affects the performance of the photovoltaic systems and the solar potential (Jochem et al. 2011; Redweik et al. 2013).

This paper proposes a solar potential estimation for the most suitable roof surfaces. The topographic data is obtained from LiDAR, which stands for Light Detection and Ranging (Le et al. 2016). The time-dependent solar irradiance is estimated using statistical data from Photovoltaic Geographical Information System (PVGIS), (European Commission, Joint Research Centre 2019) measurements of global irradiances that provide a free and open web

---

Analysis of solar potential in an urban area using LiDAR data: A case study of Belgium (10870)
Sharareh Akbarian (Australia), Arash Jouybari and Nina Grondstein (Sweden)

FIG e-Working Week 2021
Smart Surveyors for Land and Water Management - Challenges in a New Reality
Virtually in the Netherlands, 21–25 June 2021

access map-based inventory of solar energy resource and assessment of the electricity generation from photovoltaic systems in Europe, Africa, and South-West Asia. To accurately estimate the solar potential, the obtained instantaneous solar irradiance is reduced by considering the roofs' locations, the influences of cloud cover and atmospheric scattering (i.e. splitting the irradiance into diffuse and direct components), surface inclination and orientation, and shadowing caused by nearby objects (e.g. buildings and vegetation)j(Brito et al. 2017).

The solar potential estimation in the previous studies includes three important phases. The first phase involves building segmentation and extraction. There are two main approaches for building extraction from laser scanning data such as LiDAR. In most cases, building detection is performed on aggregated 2.5D grid data, which reduces the amount of the 3D LiDAR point cloud and makes processing less time-consuming by using a regular data model. Therefore, the complexity of the 3D space has not been considered anymore but is irreversibly lost. When a Digital Terrain Model (DTM) is subtracted from a Digital Surface Model (DSM), a normalized Digital Surface Model (nDSM) is generated which is utilized to detect buildings based on a 2.5D grid data (Bizjak et al. 2015; Gooding et al. 2015; Kassner et al. 2009; Le et al. 2016; Lukač and Žalik 2013; Redweik et al. 2013).

Other authors have identified buildings from the original point cloud of LiDAR and extraction of the roofs and the calculation of the slope and aspect of each roof are implemented directly on the LiDAR point cloud (Huang et al. 2012; Jacques et al. 2014; Margolis et al. 2017). However, all the mentioned studies have employed low-resolution LiDAR data. Other methods use planar patches and automatically selecting seed points by nit normal of triangles which are mapped onto a Gauss Sphere (Cao et al. 2017). Another approach involves clustering by fuzzy c-means for roof detecting and region growing algorithm for segmenting roofs (Albano 2019). Building roof edges can also be extracted from LiDAR data by combining an adapted version of RanSAC (random sample consensus) line fitting with DBSCAN Density-Based Spatial Clustering of Applications with Noise) (Widyaningrum et al. 2018).

In the second phase, the shadow of the neighboring and adjacent sides of each rood surface must be calculated for each time according to the position of the sun and the objects surrounding the surface. In several studies, the shadow effects, in general, have not been taken into account in calculating output (Huang et al. 2012; Le et al. 2016; Szabó et al. 2016; Vögtle et al. 2005). Therefore, the result of such work is not adequate. Others have used the original point cloud of LiDAR data directly to examine the shadow (Brito et al. 2017; Jochem et al. 2009a; Jochem et al. 2011; Margolis et al. 2017). In this approach, the required values for the input of the shadow algorithm are the position of the sun at any given time. At a specific distance in the direction of the sun's azimuth from a selected roof surface to the sun, all existing points are extracted from LiDAR data. Next, the elevation of those points is compared with the elevation of the sun and the elevation of the selected roof surface to detect the shadow. In some studies, the same method is used but using a DTM in computations instead (Lukač and Žalik 2013; Redweik et al. 2013).

In previous studies, three main methods were found in the final phase of calculating the solar potential for the obtained roof surfaces via the previous phases. The first method uses the same

amount of solar radiation that is considered for all the cells of roof surfaces throughout the whole day. Such a method, according to the dependence of solar radiation parameters anywhere to the time, latitude, longitude, and shadow, does not produce reliable results and can be used only as an initial value. The second method includes using solar radiation data from the National Renewable Energy Laboratory (SOLPOS code), which gives the amount of direct and diffuse radiation incidents for every hour and cell of the grid (Brito et al. 2017; Jochem et al. 2009a; Jochem et al. 2011; Lukač et al. 2013). The third one considers the cloudiness conditions of the sky for the diffuse radiation in the calculations (Jakubiec and Reinhart 2012; Redweik et al. 2013).

2. PROPOSED METHOD

In this paper, an idea is proposed to extract the major roof surfaces of the buildings which are potentially suitable for photovoltaic systems from LiDAR data. Then an identification value of potential solar in a year will be obtained for the installation of the photovoltaic systems. The workflow of the proposed algorithm is illustrated in *Fig 1*.
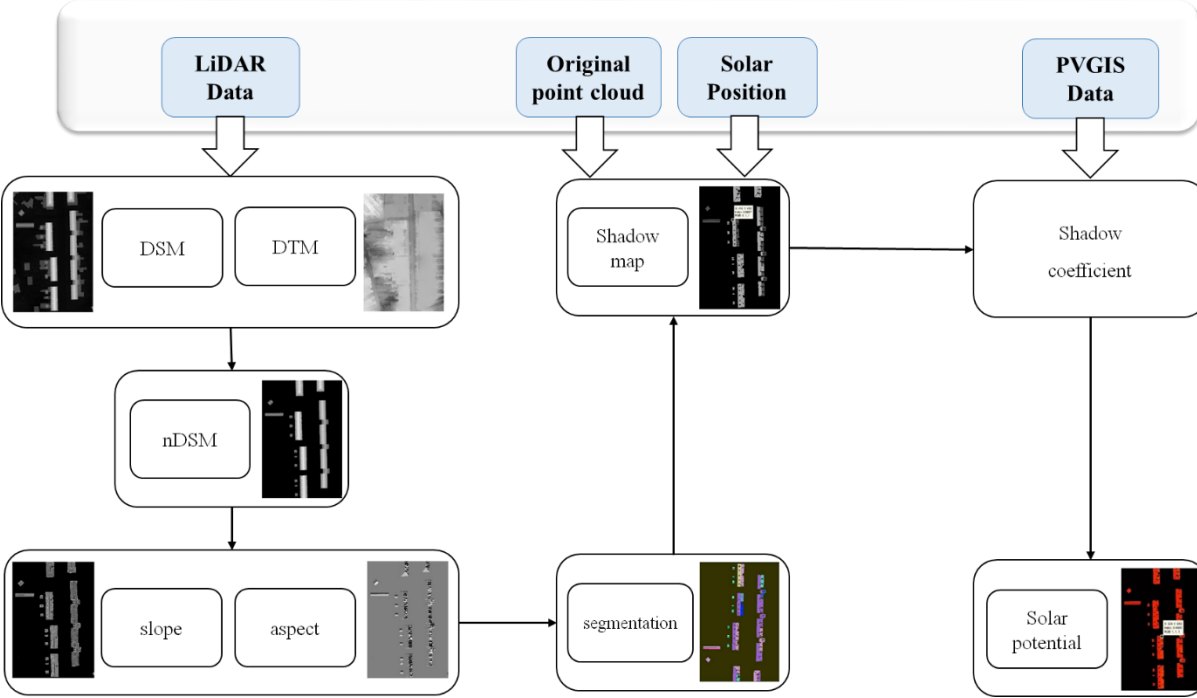
Figure 1. The workflow of the proposed approach

Analysis of solar potential in an urban area using LiDAR data: A case study of Belgium (10870)
Sharareh Akbarian (Australia), Arash Jouybari and Nina Grondstein (Sweden)

FIG e-Working Week 2021
Smart Surveyors for Land and Water Management - Challenges in a New Reality
Virtually in the Netherlands, 21–25 June 2021

2.1 Generating nDSM

Major 3D models can be extracted by LiDAR data. A DSM is an elevation model that includes man-made and natural objects such as buildings, trees, and powerlines. While a DTM is an elevation model representing the bare earth surface without any kind of natural and artificial objects like houses, towers, or bridges (Arefi 2007; Arefi and Hahn 2005). The nDSM is created by subtracting the DTM value from the DSM grid.

2.2 Calculating slope and aspect

The essential factors for filtering the roof surfaces are slope and aspect (*Fig 2*). The slope and aspect angles are calculated for each cell of nDSM by the surface normal vector. First, the normal vector of each cell in the nDSM grid is calculated. Afterward, the slope is obtained as the angle between the upward vector of the horizontal plane and the normal vector of the cells (Eq1) (Jacques et al. 2014).

$$Slope = \tan^{-1}(Normal\ z / \sqrt{(Normal\ x)^2 + (Normal\ y)^2}\ ) \qquad (1)$$

The aspect is the angle between the projected points of the normal vector on the horizontal plane and the vector directed towards the geographical north. The related equation is provided below (Eq (2)) (Jacques et al. 2014).

$$Aspect = \tan^{-1}(Normal\ y / (-Normal\ x)) \qquad (2)$$

Analysis of solar potential in an urban area using LiDAR data: A case study of Belgium (10870)
Sharareh Akbarian (Australia), Arash Jouybari and Nina Grondstein (Sweden)

FIG e-Working Week 2021
Smart Surveyors for Land and Water Management - Challenges in a New Reality
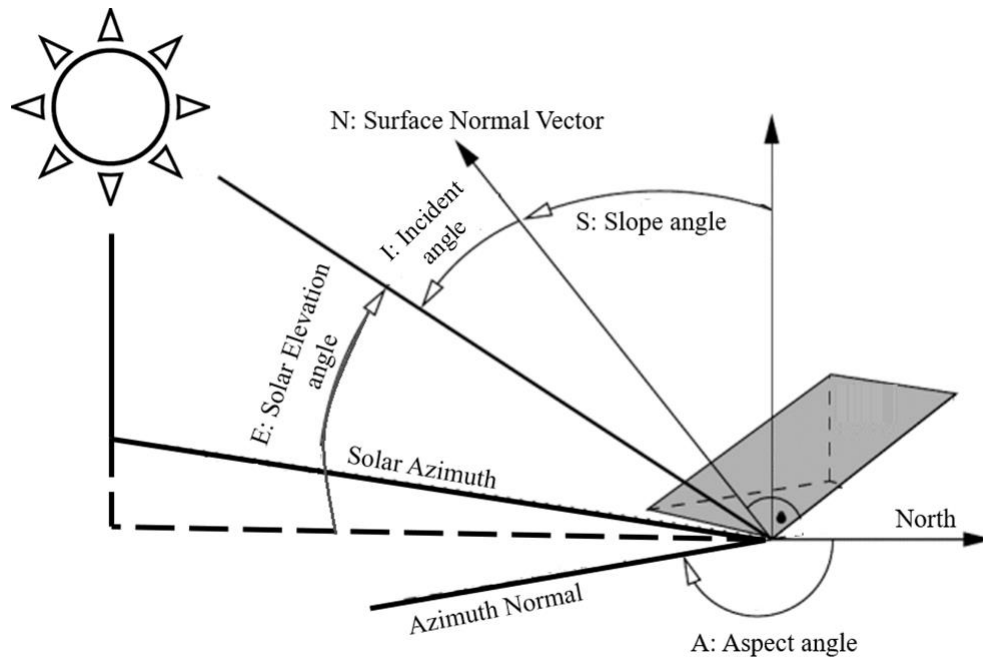Virtually in the Netherlands, 21–25 June 2021

Figure 2. Slope and Aspect angles (Neteler and Mitasova 2008)

2.3 Segmentation based on slope, aspect, and height

The roof surfaces of the buildings are divided into two categories, tilted and flat. If the slope of a roof is less than 10 degrees, it is a flat roof and thus the tilted roof has a slope between 10 to 65 degrees, based on the prevailing percentage of roofs in the region (Huang et al. 2012; Kassner et al. 2009). Flat roofs are segmented by height and tilted roofs are segmented by slope and aspect. Each cell in the same flat roof surface possesses a similar slope, aspect, and height, while each cell in the same tilted roof surface possesses a similar slope and aspect. A region-growing algorithm followed by a series of operation such as object identification, morphological operation (Luhmann et al. 2013), and boundary facing is applied to segment the roof surfaces according to the factors of the slope, aspect, and height (this refers to the height of an object above the ground surface) derived from nDSM. The region growing approach is applied in which adjacent cells are grouped with the same domain to form a partitioned region. The segmentation begins by randomly selecting a set of fundamental points on the roof's buildings. The points adjacent to the fundamental point are compared in height. If they have zero difference, they are in the same group and are considered flat roofs. Otherwise, region growing is performed by integrating the points adjacent to each point of the site, which has a certain range of two slope and aspect values. Grouped surfaces are in the category of tilted roofs. The segmented roof surfaces possess specific attributes, including roof plan area, average slope, and aspect, providing valuable indications to further analyze suitable locations for receiving solar energy.

Analysis of solar potential in an urban area using LiDAR data: A case study of Belgium (10870)
Sharareh Akbarian (Australia), Arash Jouybari and Nina Grondstein (Sweden)

FIG e-Working Week 2021
Smart Surveyors for Land and Water Management - Challenges in a New Reality
Virtually in the Netherlands, 21–25 June 2021

2.4 Selection of appropriate locations for the installation of the photovoltaic system

After segmentation, it is necessary to evaluate the area, slope, aspect, and shadow of segments to identify whether the segments are suitable for photovoltaic systems installation or not. Then the solar potential rating list is constructed for those segments that have not been filtered out. Segments are selected according to their orientation towards the equator. As the study area is located in the Northern hemisphere, segments in south, southeast, and southwest directions will receive higher solar energy (Huang et al. 2012). Moreover, protected areas within the city (e.g. cultural heritage buildings) and small segmented areas on the roofs such as chimneys or windows should be removed.

2.5 Shadow Detection Methodology

The use of a constant solar radiation value across a roof surface during different times will be inaccurate because a constant value does not consider trees and neighboring buildings which shade the building roofs and the elevation and azimuth of the sun's effect. Solar radiation on the earth's surface is composed of the sum of direct and diffuse sunlight; therefore, it is essential to determine if a particular spot receives direct sunlight or if it is in shadow at a particular time. The shadow at different times and places vary due to the difference in azimuth and elevation solar angles. The elevation angle is the angular height of the sun in the sky measured from the horizon. Note that, both altitude and elevation are also used to describe the height in meters above sea level. The elevation is 0° at sunrise and 90° when the sun is directly overhead. The elevation angle varies throughout the day. It also depends on the latitude of a particular location and the day of the year. An important parameter in the design of photovoltaic systems is the maximum elevation angle that is the maximum height of the sun in the sky at a particular time of year. The azimuth angle is the compass direction from which the sunlight is coming. The azimuth angle varies throughout the day in a year.

The selected segments must first be masked into the original point cloud of LiDAR data to evaluate the effect of shadows on the selected roof surfaces. Due to the conversion of the original point cloud to the DSM grid, much of the three-dimensional information is lost. As a result, for a more accurate study of the shadows, it is preferable to use the original LiDAR point cloud. The center of gravity (x, y) on the original LiDAR point cloud for each roof surface is approximated using the DSM model. The position of the sun on each day of the year is obtained using the coordinates of this center, which includes the sun's elevation and azimuth angle. Then the direction of the sun's azimuth - the vector from the sun's position to the given point's position is searched along a specified distance (D) to find any existing object as the object (X, Y). As shown in Eq 3, 4.

$$X = x + D * \sin(\ solarazimuth) \qquad (3)$$
$$Y = y + D * \cos(\ solarazimuth) \qquad (4)$$

Analysis of solar potential in an urban area using LiDAR data: A case study of Belgium (10870)
Sharareh Akbarian (Australia), Arash Jouybari and Nina Grondstein (Sweden)

FIG e-Working Week 2021
Smart Surveyors for Land and Water Management - Challenges in a New Reality
Virtually in the Netherlands, 21–25 June 2021

For found objects, their elevation was derived from the DSM and compared against the elevation of the sun considering the sun positions at different times of the year. If the elevation of the sun will be higher than the elevation of the obstacle object, the desired point will not be in the shadow and vice versa. Finally, for every roof surface, a shadow coefficient between 0 and 1 is obtained. The value of 1 means that the roof surface is completely in the shadow whereas the value of 0 means that the roof surface is not in the shadow.

2.6 Solar Potential

The time-dependent solar irradiance is estimated through Eq.5 by using statistical data derived from PVGIS measurements of global irradiances. The amounts of direct (I_{pb}) and diffuse (I_{pd}) radiation in a year is obtained from PVGIS (Lukač et al. 2013).

$$I_p = I_{pb}\left(1 - S_p\right) + I_{pd} \tag{5}$$

In Eq.5, the shadowing coefficient (S_p) is considered, thus fully shadowed points ($S_p = 1$) receive only diffuse radiation. Areas that are partially shadowed, receive reduced amounts of direct irradiance. In this equation, p represents the candidate cell per roof surface. The amount of I_p for each day by using a specified time-step as three times per day is calculated. Eq 6 is used to calculate the average of I_p in each season for each cell. In this equation, n refers to time steps. The solar potential P_p is defined as its seasonal insolation, which is calculated as the average daily insolation throughout the season as shown in Eq. 7. In this equation, I_{Tp} stands for the average amount of I_p for each season, and the maximum amount among the seasons will be considered as $max\left(I_{Tp}\right)$. After solar potential calculations, the segments are categorized within a rating list consisting of four categories as Table(1).

$$I_{Tp} = \frac{\sum_{i=1}^{i=n} I_i}{n} \tag{6}$$

$$P_p = \frac{I_{Tp}}{max\left(I_{Tp}\right)} \tag{7}$$

Table 1. The rating list of solar potential

Solar potential ranges	Rating categories
P> 0.75	very high suitability
0.75>=P>0.5	high suitability
0.5>=P>0	low suitability
P = 0	unsuitable

Analysis of solar potential in an urban area using LiDAR data: A case study of Belgium (10870)
Sharareh Akbarian (Australia), Arash Jouybari and Nina Grondstein (Sweden)

FIG e-Working Week 2021
Smart Surveyors for Land and Water Management - Challenges in a New Reality
Virtually in the Netherlands, 21–25 June 2021

3. STUDY AREA AND DATA

The study area is located in Zee Bruges, Belgium in Europe. The total area is covered with the extremely high-resolution LiDAR and optical data that is provided by the 2015 IEEE GRSS data fusion contest, organized by the Image Analysis and Data Fusion Technical Committee (2015) (*Fig 3*). The LiDAR grid data has a point spacing of 10 cm and has been produced from a point cloud with a point density of ~65 points/m². Additionally, one color orthophoto with a 5 cm spatial resolution is also provided (*Fig 3*). They cover an urban and harbor area in Zee Bruges, Belgium, and were acquired and provided for the Contest by the Belgian Royal Military Academy. As a test area, a rectangular section (3000 m* 2000 m) of an urban area (*Fig 4*) is selected as it contains single buildings as well as building rows and blocks.

Figure 3. Optical Data and DSM (Low areas are represented in black and scale to the highest areas in white).

Analysis of solar potential in an urban area using LiDAR data: A case study of Belgium (10870)
Sharareh Akbarian (Australia), Arash Jouybari and Nina Grondstein (Sweden)

FIG e-Working Week 2021
Smart Surveyors for Land and Water Management - Challenges in a New Reality
Virtually in the Netherlands, 21–25 June 2021

Figure 4. The selected area

4. RESULTS AND DISCUSSION

In this paper, an approach to determine and select suitable roof areas for photovoltaics is presented. The calculation of the suitability of areas for Photovoltaic system installation is an important goal of this work.
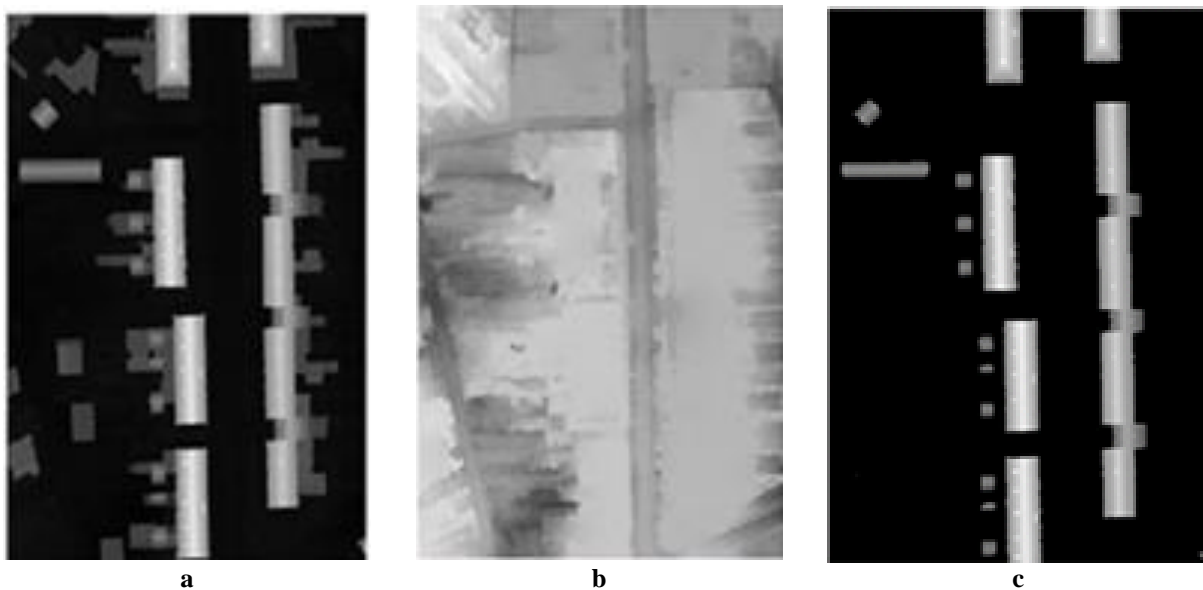

| a | b | c |

Figure 5. Creation of a nDSM: **a**) DSM, **b**) DTM and **c**) nDSM (Low areas are represented in black and scale to the highest areas in white)

The first step of the proposed approach concentrates on providing the nDSM from the DSM and DTM. *Fig 5* demonstrates the nDSM as the result of the DSM and DTM on the selected area. In the second step of the procedure, the surface normal vector for each point in the cell was calculated from the nDSM to determine the slope and aspect. There were three outputs for the normal vector on the surface in the three directions x, y, and z. Eqs (1) and (2) were applied to provide slope and aspect of the experimental data. *Fig 6* shows the results of these two features in the selected area. The area of the slope map (*Fig* 6.a) in white indicates the steeper area and the darker the color, the flatter the terrain.

Analysis of solar potential in an urban area using LiDAR data: A case study of Belgium (10870)
Sharareh Akbarian (Australia), Arash Jouybari and Nina Grondstein (Sweden)

FIG e-Working Week 2021
Smart Surveyors for Land and Water Management - Challenges in a New Reality
Virtually in the Netherlands, 21–25 June 2021

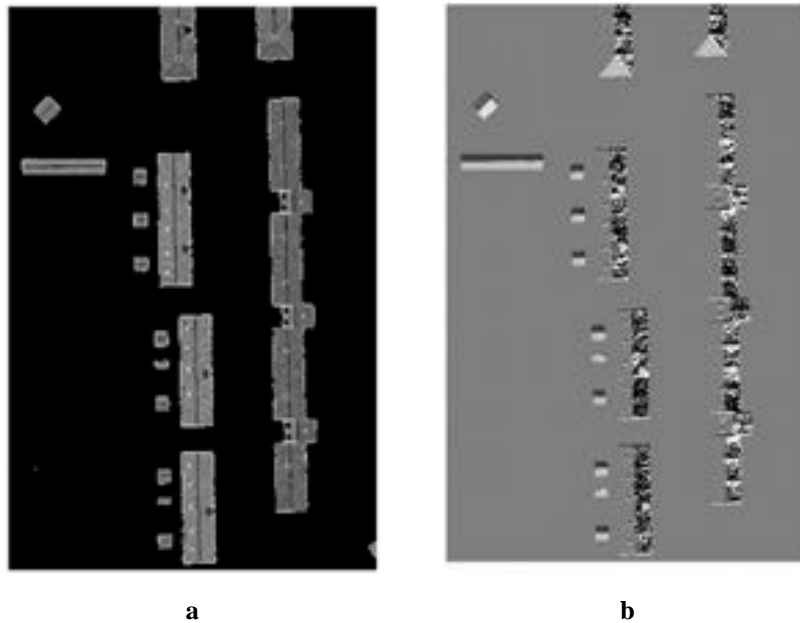a   b

Figure 6. Calculation of slope and aspect **a**) slope and **b**) aspect

Thirdly, in this area, any historical buildings were excluded by visual assessment of the optical image. All extracted roofs had an appropriate range between 30 and 65 degrees in terms of the slope. In terms of aspect, they had the right conditions for the installation of photovoltaic devices. A filter area had been taken to remove surfaces with an area of less than 5 square meters.

Next, the region growing approach was applied in which adjacent pixels with similar features were grouped to form a partitioned region. The process had been applied through MATLAB programming (The MathWorks, Inc. 2018). The threshold for the slope and aspect was determined by the user based on the prevailing percentage of roofs in the region. Regardless of the type of area, there was no flat roof type, and all the roof surfaces were sloped. After this step, each roof of the building varied with different slopes and aspects (*Fig.* 7). In this figure, each segment had been determined with a unique color. (Chaves and Bahill 2010).

Analysis of solar potential in an urban area using LiDAR data: A case study of Belgium (10870)
Sharareh Akbarian (Australia), Arash Jouybari and Nina Grondstein (Sweden)

FIG e-Working Week 2021
Smart Surveyors for Land and Water Management - Challenges in a New Reality
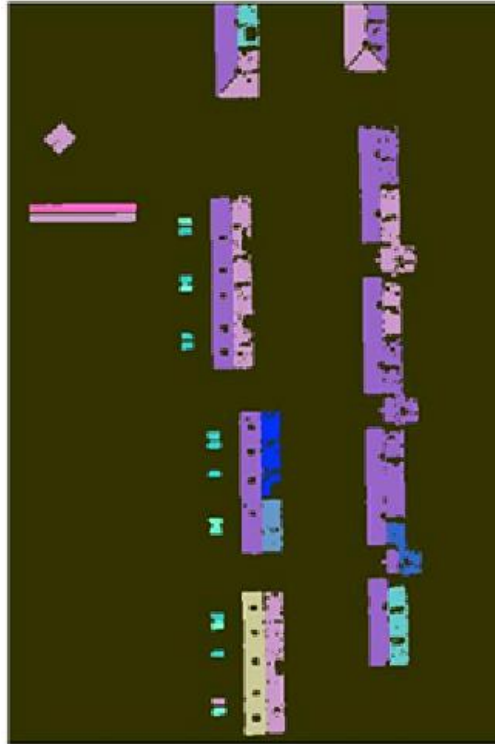Virtually in the Netherlands, 21–25 June 2021

Figure 7. Segmented roofs in region growing algorithm

After segmenting the roof surfaces based on the slope, aspect, and height, the proposed method focused on the most important phase of this work, which is the shadow detection algorithm. The shadow contains the shadow of the nearby effects, the shadow of the terrain, and the shadow of the plants. Firstly, the segments generated by the region growing algorithm on an irregular 3D point cloud of the LiDAR are masked to determine the amount of shadow on each surface and in each season of the year. For the center of gravity of each segment, the geographical coordinates of all existing objects along a constant distance of 15 m were calculated using Eqs (3) and (4). The elevation of all these objects was compared with the elevation of the desired segment and sun. If the desired segment is higher than the sun's elevation, the roof surface is in the shadow. This process was calculated three times per day for the year. In the end, the shadow values were averaged over a day and every three months of the season and reached the final number for the amount of shadow throughout each season, as shown in *Fig 8*.

Analysis of solar potential in an urban area using LiDAR data: A case study of Belgium (10870)
Sharareh Akbarian (Australia), Arash Jouybari and Nina Grondstein (Sweden)

FIG e-Working Week 2021
Smart Surveyors for Land and Water Management - Challenges in a New Reality
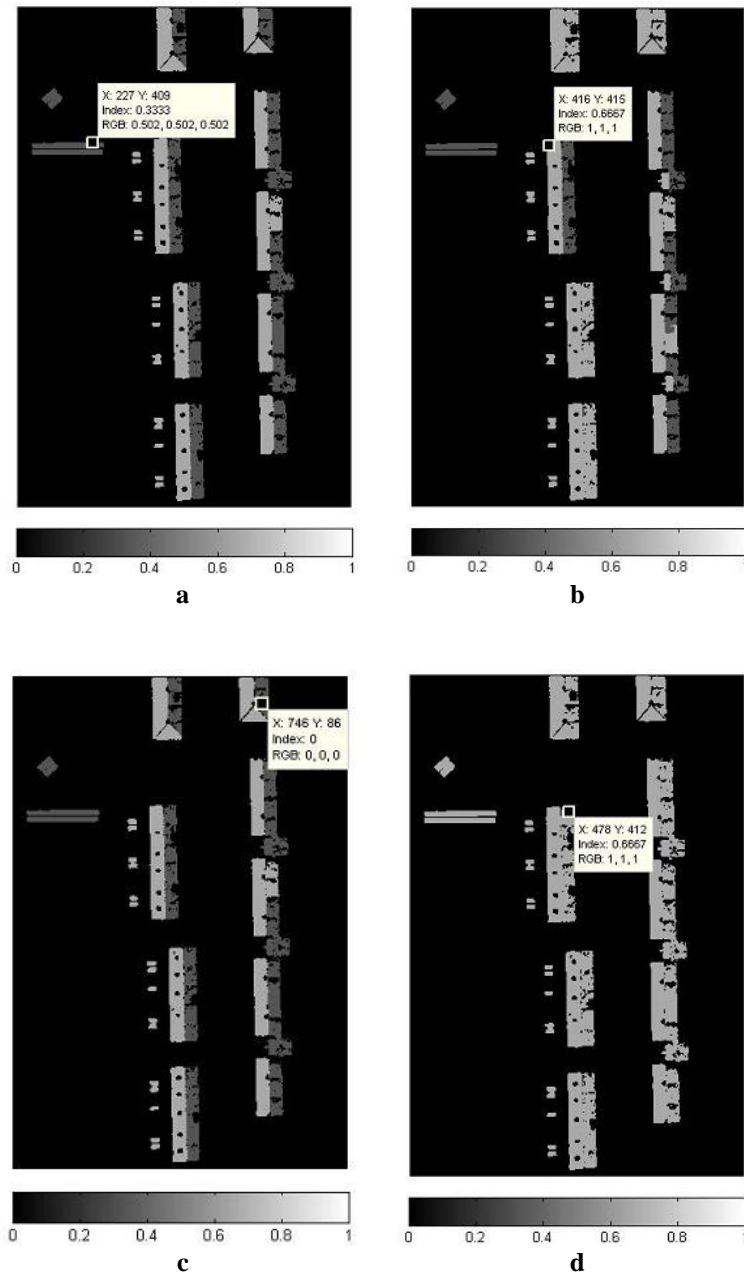Virtually in the Netherlands, 21–25 June 2021

Figure 8. Shadow of different seasons: **a**) spring, **b**) summer, **c**) autumn, and **d**) winter

The resulting value is a shadow indicator at the desired level at that time to have the minimum amount of the shadow. As the shadow factor approaches zero, the amount of shadow is reduced. Finally, for appropriate roof surfaces, the received solar energy was calculated using Eq (3) three times (morning, noon, and afternoon) per day. The received solar energy values were averaged over a day and every three months of the season, and they reached the final figure for the amount of solar energy received during each season. By having the maximum received

Analysis of solar potential in an urban area using LiDAR data: A case study of Belgium (10870)
Sharareh Akbarian (Australia), Arash Jouybari and Nina Grondstein (Sweden)

FIG e-Working Week 2021
Smart Surveyors for Land and Water Management - Challenges in a New Reality
Virtually in the Netherlands, 21–25 June 2021

amount of solar energy at each roof surface, the amount of solar energy received per roof surface per season was based on a number between zero and one as shown in Eq (7). As shown in *Fig 9*, all surfaces in summer have the most solar energy. As a result, the solar potential number is one for them.
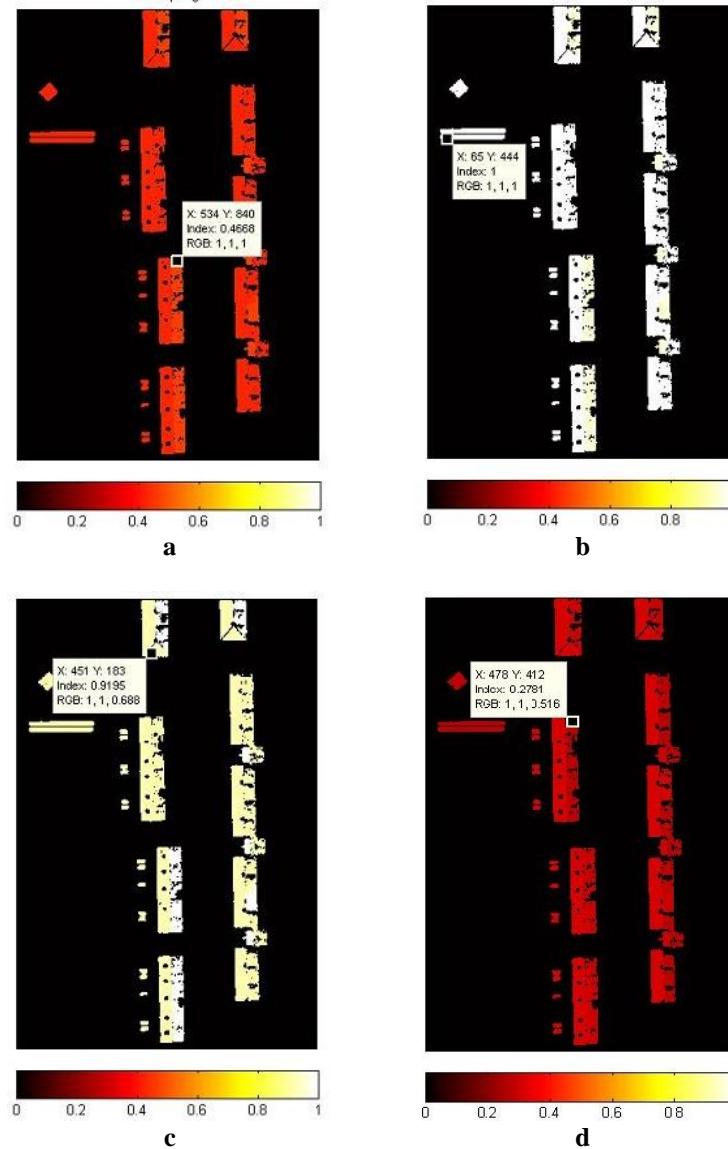

Figure 9. Solar potential: **a**) spring, **b**) summer, **c**) autumn, and **d**) winter

Based on the output of the segmentation process, there were 50 surfaces of the roof (*Fig* 10). In Table (2), for each surface, the slope, the aspect, and the amount of received solar energy by considering the shadow in each season are presented. The slope values were in the range of [0-

Analysis of solar potential in an urban area using LiDAR data: A case study of Belgium (10870)
Sharareh Akbarian (Australia), Arash Jouybari and Nina Grondstein (Sweden)

FIG e-Working Week 2021
Smart Surveyors for Land and Water Management - Challenges in a New Reality
Virtually in the Netherlands, 21–25 June 2021

90] degrees and the aspect values were [0-360] degrees in the range. The division of aspect values is described in Table (3).

Table 2. Calculated specifications of each building surface

Building code	Surface code	Slope (degree)	Aspect (degree)	Spring Radiation (W / m2)	Summer Radiation (W / m2)	Fall Radiation (W / m2)	Winter Radiation (W / m2)	Surfaces
1	1	44.96	176	2788.3	6528.3	5973	1815.3	a
	2	44.02	179.76	2788.3	6528.3	5973	1815.3	
2	1	39.33	292.65	2788.3	6528.3	5973	1815.3	b
	2	38.11	141.43	2788.3	6528.3	5973	1815.3	
3	1	39.95	170.3	2788.3	6528.3	5973	1815.3	c
	2	39.15	177.77	2788.3	6528.3	5973	1815.3	
4	1	39.27	181.28	2788.3	6528.3	5973	1815.3	d
	2	39.96	179.41	2788.3	6528.3	5973	1815.3	
5	1	39.27	178.06	2452.7	5712.7	5253	1815.3	e
	2	39.69	177.11	2452.7	5712.7	5253	1815.3	
6	1	39.93	184	2452.7	5712.7	5253	1815.3	f
	2	38.64	177.57	2452.7	5712.7	5253	1815.3	
7	1	39	179.09	2452.7	5712.7	5253	1815.3	g
8	1	37.5	192.03	2452.7	5712.7	5253	1815.3	h
	2	37.2	180.43	2452.7	5712.7	5253	1815.3	
9	1	42.34	253.75	2452.7	5712.7	5253	1815.3	i
	2	43.99	90.39	2778.3	6528.3	5973	1815.3	
	3	43.31	91.3	2778.3	6528.3	5973	1815.3	
10	1	38.9	167.79	2452.7	5712.7	5253	1815.3	j
	2	37.71	178.35	2452.7	5712.7	5253	1815.3	
11	1	38.28	179.24	2452.7	5712.7	5253	1815.3	k
12	1	42.25	203.41	2452.7	5712.7	5253	1815.3	l
	2	39.2	179.98	2452.7	5712.7	5253	1815.3	
13	1	37.64	258.76	2452.7	5712.7	5253	1815.3	m
	2	36.76	170.56	2452.7	5712.7	5253	1815.3	
	3	38.39	90.86	2778.3	6528.3	5973	1815.3	
	4	38.85	88.91	2778.3	6528.3	5973	1815.3	
14	1	41.18	254.38	2452.7	5712.7	5253	1815.3	n
	2	42.96	94.67	2778.3	6528.3	5973	1815.3	
	3	43.39	90.31	2778.3	6528.3	5973	1815.3	
15	1	42.86	254.19	2452.7	5712.7	5253	1815.3	o
	2	43.16	91.76	2778.3	6528.3	5973	1815.3	
16	1	39	260.94	2452.7	5712.7	5253	1815.3	p
	2	35.48	178.92	2452.7	5712.7	5253	1815.3	
17	1	34.6	255.78	2452.7	5712.7	5253	1815.3	q
	2	34.27	255.3	2452.7	5712.7	5253	1815.3	
	3	35.11	253.91	2452.7	5712.7	5253	1815.3	
	4	34.57	255.01	2452.7	5712.7	5253	1815.3	
	5	33.55	93.03	2778.3	6528.3	5973	1815.3	
	6	35.26	247.97	2778.3	6528.3	5973	1815.3	
	7	33.57	92.89	2778.3	6528.3	5973	1815.3	
	8	34.57	90.82	2452.7	5712.7	5253	1815.3	
	9	33.89	93.93	2778.3	6528.3	5973	1815.3	
	10	38	257.78	2778.3	6528.3	5973	1815.3	
	11	35.61	246.61	2778.3	6528.3	5973	1815.3	
	12	33.69	92.81	2778.3	6528.3	5973	1815.3	
	13	34.6	90.06	2778.3	6528.3	5973	1815.3	
	14	33.88	90.92	2778.3	6528.3	5973	1815.3	
	15	34.15	92.84	2778.3	6528.3	5973	1815.3	

Figure 10. The surfaces of the segmented roofs

Analysis of solar potential in an urban area using LiDAR data: A case study of Belgium (10870)
Sharareh Akbarian (Australia), Arash Jouybari and Nina Grondstein (Sweden)

FIG e-Working Week 2021
Smart Surveyors for Land and Water Management - Challenges in a New Reality
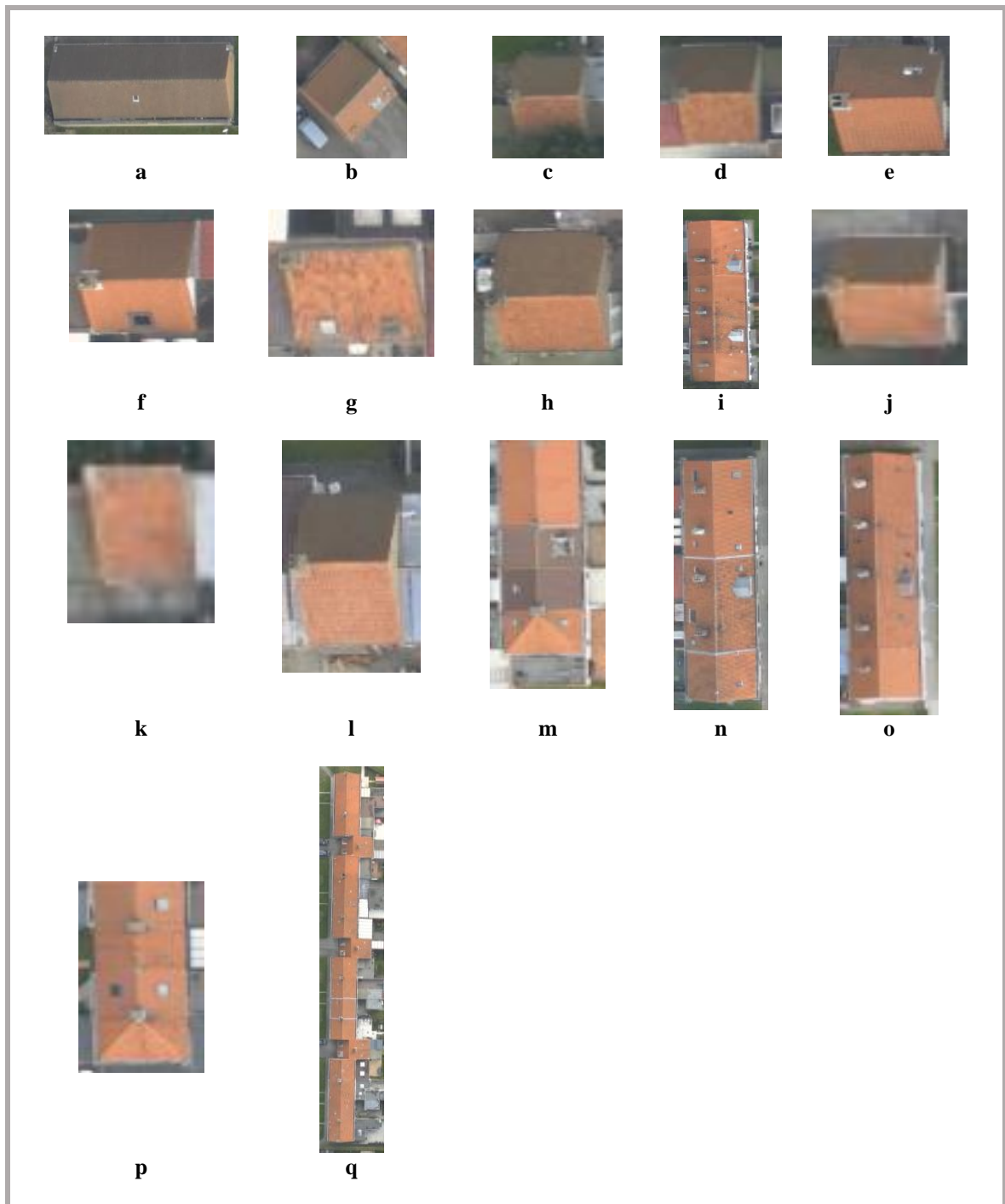Virtually in the Netherlands, 21–25 June 2021

Table 3. Description of aspect values

Direction	Value (*degree*)
North	0-22.5
Northeast	22.5-67.5
East	67.5-122.5
Southeast	122.5-157.5
South	157.5-202.5
Southwest	202.5-247.5
West	247.5-292.5
Northwest	292.5-337.5
North	337.5-360

As mentioned before, the areas in the Northern Hemisphere have the highest solar energy in the direction of southwest, south, and southeast. Based on the proposed method, the maximum and minimum amount of solar energy in each season has been studied in terms of the slope and aspect values for the desired roof. In all seasons, solar energy is the highest in the southeastern direction, and the lowest amount of solar energy is toward the southeast.

5. CONCLUSION

In this research, the proposed method was applied to a metropolitan area located in Zee Bruges, Belgium using high-resolution LiDAR data. The purpose was to determine a suitability ranking list for roof surfaces of the buildings to install the solar photovoltaic devices. For this purpose, the total roofs of the existing buildings in the selected area have been analyzed and filtered for slope, aspect, and area. Regarding the high-resolution LiDAR data, different types of roofs are successfully extracted. As an outcome, the amount of solar energy received over a given year has been calculated by taking into account the shadow and based on the total amount of solar potential in each season. Based on the high-resolution 3D point cloud of LiDAR, the shadow accuracy of the method is improved by considering the shadow effects created by the surrounding area and neighboring objects.

Future works should focus on the overall assessment of the solar potential on roof surfaces and vertical walls together for receiving a maximum solar potential in all seasons of a year. Because dust and snow are less absorbed by the vertical walls compared to the roof surfaces due to their vertical slope (Redweik et al. 2013). The vertical walls also have at least two surfaces with opposite directions which can absorb the maximum solar energy at different times of the day (Redweik et al. 2013). On the other hand, the roof surfaces of the buildings have less shading and more useful area for the installation of photovoltaic solar converters. However, aerial LIDAR data is not suitable for the assessment of the solar potential on the vertical walls due to the high laser inclination angle, the aircraft position relative to the buildings, and the limitation of laser returns from the vertical walls of buildings. Therefore, a combination of aerial and

Analysis of solar potential in an urban area using LiDAR data: A case study of Belgium (10870)
Sharareh Akbarian (Australia), Arash Jouybari and Nina Grondstein (Sweden)

FIG e-Working Week 2021
Smart Surveyors for Land and Water Management - Challenges in a New Reality
Virtually in the Netherlands, 21–25 June 2021

terrestrial laser scanner data could provide this opportunity to improve this method such as Liang et al. (2018) who combined UAV image data terrestrial laser scanning data, in contrast to Jochem et al. (2011) or Huang et al. (2017), who only used terrestrial scan data in their study.

Analysis of solar potential in an urban area using LiDAR data: A case study of Belgium (10870)
Sharareh Akbarian (Australia), Arash Jouybari and Nina Grondstein (Sweden)

FIG e-Working Week 2021
Smart Surveyors for Land and Water Management - Challenges in a New Reality
Virtually in the Netherlands, 21–25 June 2021

REFERENCES

Albano R (2019) Investigation on Roof Segmentation for 3D Building Reconstruction from Aerial LIDAR Point Clouds. Applied Sciences 9:4674. https://doi.org/10.3390/app9214674

Arefi H (ed) (2007) Automatic Dtm Generation From Laser-Scanning Data in Residential Hilly Area. International Archives of the Photogrammetry, Remote Sensing and Spatial Information Sciences

Arefi H, Hahn M (eds) (2005) A morphological reconstruction algorithm for separating off-terrain points from terrain points in laser scanning data, vol 36

Assouline D, Mohajeri N, Scartezzini J-L (2017) Quantifying rooftop photovoltaic solar energy potential: A machine learning approach. Solar Energy 141:278–296. https://doi.org/10.1016/j.solener.2016.11.045

Bizjak M, Žalik B, Lukač N (2015) Evolutionary-driven search for solar building models using LiDAR data. Energy and Buildings 92:195–203. https://doi.org/10.1016/j.enbuild.2015.01.051

Brito MC, Freitas S, Guimarães S, Catita C, Redweik P (2017) The importance of facades for the solar PV potential of a Mediterranean city using LiDAR data. Renewable Energy 111:85–94. https://doi.org/10.1016/j.renene.2017.03.085

Cao R, Zhang Y, Liu X, Zhao Z (2017) Roof plane extraction from airborne lidar point clouds. International Journal of Remote Sensing 38:3684–3703. https://doi.org/10.1080/01431161.2017.1302112

Chaves A, Bahill AT (2010) Locating sites for photovoltaic solar panels: Pilot study uses DEM derived from LiDAR. Energy Saving Trust 13

European Commission, Joint Research Centre (2019) Photovoltaic Geographical Information System (PVGIS). European Commission. https://ec.europa.eu/jrc/en/pvgis

Gooding J, Crook R, Tomlin AS (2015) Modelling of roof geometries from low-resolution LiDAR data for city-scale solar energy applications using a neighbouring buildings method. Applied Energy 148:93–104. https://doi.org/10.1016/j.apenergy.2015.03.013

Huang Y, Yu B, Hu Z, Wu J, Wu B (2012) Locating suitable roofs for utilization of solar energy in downtown area using airborne LiDAR data and object-based method: A case study of the Lujiazui region, Shanghai. In: Weng Q (ed) 2012 Second International Workshop on Earth Observation and Remote Sensing Applications (EORSA): 8 - 11 June 2012, Shanghai, China. IEEE, Piscataway, NJ, pp 322–326

Huang P, Cheng M, Chen Y, Zai D, Wang C, Li J (2017) Solar Potential Analysis Method Using Terrestrial Laser Scanning Point Clouds. IEEE J. Sel. Top. Appl. Earth Observations Remote Sensing 10:1221–1233. https://doi.org/10.1109/JSTARS.2016.2636300

Image Analysis and Data Fusion Technical Committee (2015) Orthophoto, DSM (GeoTIFF), Point Cloud (XYZI)

Jacques DA, Gooding J, Giesekam JJ, Tomlin AS, Crook R (2014) Methodology for the assessment of PV capacity over a city region using low-resolution LiDAR data and application to the City of Leeds (UK). Applied Energy 124:28–34. https://doi.org/10.1016/j.apenergy.2014.02.076

Jakubiec JA, Reinhart CF (2012) Towards validated urban photovoltaic potential and solar radiation maps based on LiDAR measurements, GIS data and hourly daysim simulations

Jochem A, Höfle B, Rutzinger M, Pfeifer N (2009a) Automatic roof plane detection and analysis in airborne lidar point clouds for solar potential assessment. Sensors (Basel) 9:5241–5262. https://doi.org/10.3390/s90705241

Analysis of solar potential in an urban area using LiDAR data: A case study of Belgium (10870)
Sharareh Akbarian (Australia), Arash Jouybari and Nina Grondstein (Sweden)

FIG e-Working Week 2021
Smart Surveyors for Land and Water Management - Challenges in a New Reality
Virtually in the Netherlands, 21–25 June 2021

Jochem A, Höfle B, Hollaus M, Rutzinger M (2009b) Object detection in airborne LIDAR data for improved solar radiation modeling in urban areas. In: Bretar F, Pierrot-Deseilligny M, Vosselman MG (eds) Proceedings of Laser scanning '09, 38 prt 3/W8, pp 1–6

Jochem A, Höfle B, Rutzinger M (2011) Extraction of Vertical Walls from Mobile Laser Scanning Data for Solar Potential Assessment. Remote Sensing 3:650–667. https://doi.org/10.3390/rs3030650

Kassner R, Koppe W, Schüttenberg T, Bareth G (2009) Analysis of the solar potential of roofs by using official LiDAR data XXXVII. Part B4:399–404

Le T, Kholdi D, Xie H, Dong B, Vega R (2016) LiDAR-Based Solar Mapping for Distributed Solar Plant Design and Grid Integration in San Antonio, Texas. Remote Sensing 8:247. https://doi.org/10.3390/rs8030247

Liang F, Yang B, Huang R, Dong Z, Li J (2018) Façade Solar Potential Analysis Using Multisource Point Cloud. Acta Geodaetica et Cartographica Sinica 47:225–233

Luhmann T, Kyle S, Böhm J, Robson S (2013) Close-range photogrammetry and 3D imaging, 2nd edn. De Gruyter textbook. De Gruyter, Berlin

Lukač N, Žalik B (2013) GPU-based roofs' solar potential estimation using LiDAR data. Computers & Geosciences 52:34–41. https://doi.org/10.1016/j.cageo.2012.10.010

Lukač N, Žlaus D, Seme S, Žalik B, Štumberger G (2013) Rating of roofs' surfaces regarding their solar potential and suitability for PV systems, based on LiDAR data. Applied Energy 102:803–812. https://doi.org/10.1016/j.apenergy.2012.08.042

Margolis R, Gagnon P, Melius J, Phillips C, Elmore R (2017) Using GIS-based methods and lidar data to estimate rooftop solar technical potential in US cities. Environ. Res. Lett. 12:74013. https://doi.org/10.1088/1748-9326/aa7225

Neteler M, Mitasova H (2008) Open source GIS: A GRASS GIS approach, 3rd edn. Springer, New York, NY

Redweik P, Catita C, Brito M (2013) Solar energy potential on roofs and facades in an urban landscape. Solar Energy 97:332–341. https://doi.org/10.1016/j.solener.2013.08.036

Szabó S, Enyedi P, Horváth M, Kovács Z, Burai P, Csoknyai T, Szabó G (2016) Automated registration of potential locations for solar energy production with Light Detection And Ranging (LiDAR) and small format photogrammetry. Journal of Cleaner Production 112:3820–3829. https://doi.org/10.1016/j.jclepro.2015.07.117

The MathWorks, Inc. (2018) MATLAB. The MathWorks Inc.

Vögtle T, Steinle E, Tóvári D (eds) (2005) Airborne laserscanning data for determination of suitable areas for photovoltaics, 36-3/W19. International Archives of the Photogrammetry, Remote Sensing and Spatial Information Sciences

Widyaningrum E, Lindenbergh RC, Gorte BGH, Zhou K (2018) Extraction of building roof edges from LiDAR data to optimize the digital surface model for true orthophoto generation. Int. Arch. Photogramm. Remote Sens. Spatial Inf. Sci. XLII-2:1199–1205. https://doi.org/10.5194/isprs-archives-XLII-2-1199-2018

Analysis of solar potential in an urban area using LiDAR data: A case study of Belgium (10870)
Sharareh Akbarian (Australia), Arash Jouybari and Nina Grondstein (Sweden)

FIG e-Working Week 2021
Smart Surveyors for Land and Water Management - Challenges in a New Reality
Virtually in the Netherlands, 21–25 June 2021

BIOGRAPHICAL NOTES

Sharareh Akbarian received her M.Sc. in surveying engineering with a specialization in photogrammetry from the University of Tehran, Iran in 2017. The thesis's emphasis was on using LiDAR data to quantify solar energy. She is now pursuing her Ph.D. at the University of New South Wales, Australia, with a focus on agricultural products monitoring using aerial and satellite imagery and machine learning. Sharareh also has six years of surveying experience, with a focus on image analysis and 3D mapping.

Arash Jouybari has graduated with an M.Sc. in geomantic engineering in the field of Geodesy-Hydrography from the University of Tehran, Iran in 2017; the M.Sc. thesis was "Field calibration of GPS/INS navigation systems". Besides, he has B.Sc. in Geomatics Engineering. He is currently a Ph.D. student at the University of Gävle, Faculty of Engineering and Sustainable Development and his research focuses is on sensor fusion in aerial mobile mapping platforms.

Nina Grondstein graduated in 2019 with an M.Sc. in geodesy and geoinformatics specialized in photogrammetry from Jade University of Applied Sciences in Oldenburg, Germany. The master thesis deals with the "Accuracy analysis of Lantmäteriets photogrammetrically derived DSM in different resolutions". She is currently working as a surveying engineer at Sweco in Stockholm, Sweden responsible for UAV photogrammetry.

CONTACTS

Sharareh Akbarian

University of New South Wales
NSW 2052
Sydney
Australia
Tel. +61 48 116 6955
Email: s.akbarian@unsw.edu.au

Arash Jouybari

University of Gävle
Kungsbäcksvägen 47
Gävle
Sweden
Tel. +46 73 748 1269
Email: arash.jouybari@hig.se

Nina Grondstein

Sweco Sverige AB
Gjörwellsgatan 22
Stockholm
Sweden
Tel. +46 70 869 02 16
Email: nina.grondstein@sweco.se

Analysis of solar potential in an urban area using LiDAR data: A case study of Belgium (10870)
Sharareh Akbarian (Australia), Arash Jouybari and Nina Grondstein (Sweden)

FIG e-Working Week 2021
Smart Surveyors for Land and Water Management - Challenges in a New Reality
Virtually in the Netherlands, 21–25 June 2021